Maximizing uniaxial tensile strain in large-area silicon-on-insulator islands on compliant substrates

R. L. Peterson[a)]
Princeton Institute for the Science and Technology of Materials, Princeton University, Princeton, New Jersey 08540 and Department of Electrical Engineering, Princeton University, Princeton, New Jersey 08544

K. D. Hobart
Naval Research Laboratory, Washington, DC 20375

H. Yin
Princeton Institute for the Science and Technology of Materials, Princeton University, Princeton, New Jersey 08540 and Department of Electrical Engineering, Princeton University, Princeton, New Jersey 08544

F. J. Kub
Naval Research Laboratory, Washington, DC 20375

J. C. Sturm
Princeton Institute for the Science and Technology of Materials, Princeton University, Princeton, New Jersey 08540 and Department of Electrical Engineering, Princeton University, Princeton, New Jersey 08544

(Received 24 November 2005; accepted 3 May 2006; published online 31 July 2006; publisher error corrected 27 September 2006)

Recently we have demonstrated a process for generating uniaxial tensile strain in silicon. In this work, we generate uniaxially strained silicon and anisotropically strained silicon germanium on insulator with strain in both ⟨100⟩ and ⟨110⟩ in-plane directions. The strain is uniform over fairly large areas, and relaxed silicon-germanium alloy buffers are not used. The magnitude of uniaxial strain generated by the process is very dependent on the in-plane crystal direction, and can be modeled accurately using the known mechanical properties of silicon and germanium. A maximum uniaxial silicon strain of 1.0% in the ⟨100⟩ direction is achieved. Numerical simulations of the dynamic strain generation process are used to identify process windows for achieving maximum uniaxial silicon strain for different structural geometries. © *2006 American Institute of Physics*. [DOI: 10.1063/1.2210810]

I. INTRODUCTION

Biaxial tensile strain has long been known to increase electron mobility, both in bulk silicon and in the two-dimensional electron gas formed in the inversion channel of *n*-channel metal-oxide-semiconductor field-effect transistors (MOSFETs).[1] Recently, attention has shifted to process-induced uniaxial strain, due to the prediction of bulk piezoresistance theory that certain types of uniaxial strain will cause greater mobility enhancement than biaxial strain.[2] Experiments have shown significant increases in *n*- and *p*-channel field-effect transistor (FET) mobilities for moderate levels of stress across a ⟨110⟩ channel, where hole mobility enhancement requires compression and electron mobility enhancement requires tension. Importantly, hole mobility enhancement persisted at high vertical field, the condition under which most FETs operate. In practice, uniaxial strain is achieved in most cases by a modification of the FET gate stack or source/drain fabrication process.[2] Such process-induced strain can be rather anisotropic and nonuniform and is limited to very short channel devices.[3] Moreover, bulk piezoresistance measurements show maximum electron mobility enhancement when tension is applied in a ⟨100⟩ direction, that is, mobility enhancement depends on the strain direction relative to crystal planes. So, the typical ⟨110⟩ alignment may not be optimal. Other strain techniques, namely, mechanical thinning and bending of the substrate[4] or strained layer transfer,[5] have been demonstrated only for low levels of strain (at most a few tenths of a percent). These methods generate a single type of strain across the whole sample, which is not ideal for mobility enhancement.

Previously we have demonstrated electron mobility enhancement in biaxially strained silicon on insulator (SOI),[6] where the strained SOI is made by a process which does not use relaxed silicon-germanium (SiGe) buffers. The strained SOI layers are made by transferring a strained SiGe cap layer (later removed) and an unstrained silicon layer to a borophosphorosilicate glass (BPSG) film that can flow at high temperatures. The SiGe strain transfers to the underlying silicon layer, a process which recently we have adapted to yield uniaxial silicon strain.[7,8] With this strain engineering method we have fabricated biaxially strained, uniaxially strained, and unstrained silicon films, with ⟨100⟩ and ⟨110⟩ orientations, all on the same sample. By integrating multiple types and direc-

[a)]Present address: Cavendish Laboratory, University of Cambridge, Cambridge CB3 0HE, UK; electronic mail: rlp38@cam.ac.uk

 © 2006 American Institute of Physics

Downloaded 02 Feb 2007 to 128.112.140.109. Redistribution subject to AIP license or copyright, see http://jap.aip.org/jap/copyright.jsp

tions of strain on a single wafer, one can, in principle, simultaneously maximize both electron and hole mobilities. In this work, we first show experimentally that the magnitude of uniaxial strain depends on crystal orientation, with a maximum observed uniaxial silicon strain of 1.0% along ⟨100⟩. We quantitatively model this dependence, which comes from the anisotropic elastic compliance constants (s_{11}, s_{12}, s_{44}) of silicon and SiGe. Second, the generation of uniaxial strain depends on relaxation and strain transfer occurring in one in-plane direction but not the other. We perform dynamic simulations of strain generation to illustrate this process and determine the process window for uniaxial strain generation with different structural geometries.

Section II presents our experimental approach for generating biaxially symmetric and asymmetric strain in SiGe-on-insulator layers and demonstrates the dependence of asymmetric strain on crystal direction. In Sec. III we study numerical models of strain generation to determine process windows for maximum asymmetry of strain, and compare model results to our data. Finally, in Sec. IV we present measurements of uniaxial strain in thin SOI films, and compare the predicted and measured crystal-direction dependence of uniaxial silicon strain.

II. GENERATION OF BIAXIALLY SYMMETRIC AND ASYMMETRIC SiGe STRAIN, AND ITS CRYSTAL DIRECTION DEPENDENCE

This section reviews our process for growing strained SiGe/unstrained silicon layers on silicon, transferring them to a compliant substrate, and allowing them to relax in a lateral direction to generate biaxially symmetric and asymmetric strain in the SiGe layer, and explores the crystal direction dependence of the asymmetric SiGe strain.

A layer of 30-nm compressively strained $Si_{0.7}Ge_{0.3}$ with a 1-nm unstrained silicon cap is pseudomorphically grown on a sacrificial silicon substrate. The SiGe is fully strained with an initial strain ε_o of −1.2%. Since the layer is thin and strained, it can be grown with very low defect densities. Using a wafer bonding and Smart-Cut™ layer transfer process,[9,10] the layers are transferred onto a silicon handle wafer coated with BPSG, and are patterned into rectangular islands. A cross section is shown in the inset of Fig. 1, where for simplicity the very thin (∼1 nm) silicon layer between SiGe and BPSG is neglected. The BPSG layer (4.4% B and 4.1% P by weight) is 1 μm thick. Upon high temperature anneal (>700 °C), the BPSG becomes soft and can flow, so the SiGe relaxes laterally to become less-compressively strained. If annealed for a sufficiently long time, the SiGe will fully relax so the film island is strain and stress free, that is $\varepsilon_{xx}=\varepsilon_{yy}=\varepsilon_{zz}=\sigma_{xx}=\sigma_{yy}=\sigma_{zz}=0$ [Fig. 2(a)], where ε_{ii} and σ_{ii} indicate component strain and stress, respectively. (In our process the SiGe film is not vertically constrained, so σ_{zz} always equals zero and ε_{zz} is determined by Hooke's law.)

For square islands the strain at the center of the island is always biaxially symmetric in the plane of the film, that is, ε_{xx} and ε_{yy} are equal [Fig. 2(a)]. Film relaxation begins at the island edge, and proceeds toward the island center. The strain at the center of a square island decays with an exponential time constant for lateral relaxation τ_L given by[11,12]

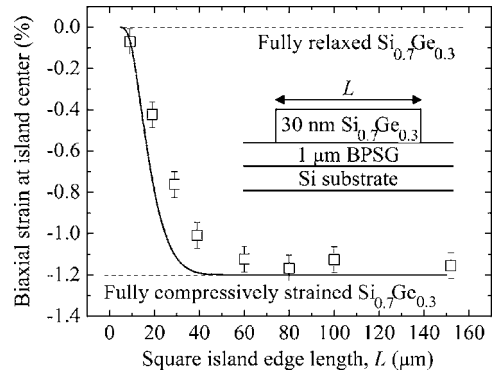

FIG. 1. Biaxial strain in SiGe layer for squares of different sizes after a 5 min anneal at 750 °C. The inset shows a schematic of the structure cross section. The thin (h_{Si}=1 nm) silicon layer between SiGe and BPSG has been omitted for simplicity. The symbols are measured biaxial strain at the island center, while the solid line depicts predicted strain at the island center, according to the model of Sec. III. The dashed lines indicate fully strained and fully relaxed $Si_{0.7}Ge_{0.3}$.

$$\tau_L = \frac{\eta L^2}{c'_{11} h_f h_g}, \tag{1}$$

where η is the viscosity of BPSG (1.2×10^{10} N s m^{-2} at 800 °C, as in Ref. 10), L the square island edge length, c'_{11} is the crystal-direction dependent SiGe film elastic stiffness coefficient (see Table I), h_f the SiGe film thickness and h_g the BPSG glass thickness. Because relaxation time depends on L^2, small islands will relax quickly, while the centers of large islands maintain their initial strain for a much longer time.[13] As shown in Fig. 1, after a 5 min anneal at 750 °C, SiGe islands of size 10×10 μm^2 are fully relaxed, while the centers of large islands (>60×60 μm^2) remain fully compressively strained with $\varepsilon_{xx}=\varepsilon_{yy}=\varepsilon_o=-1.2\%$.

Strain at the island center is measured by micro-Raman spectroscopy at 514 or 488 nm, with a spot size of ∼3 μm. From the measured peak wave number of Si–Si phonons, strain values are calculated using[14]

$$\omega_{\text{measured}} = \omega_o + \frac{\omega_o}{2}\left(q + \frac{s_{12}}{s_{11}+s_{12}}p\right)(\varepsilon_{xx}+\varepsilon_{yy}), \tag{2}$$

where ε_{xx} and ε_{yy} represent film strain in the two perpendicular in-plane directions (Fig. 2). Values for the other parameters are given in Table I.

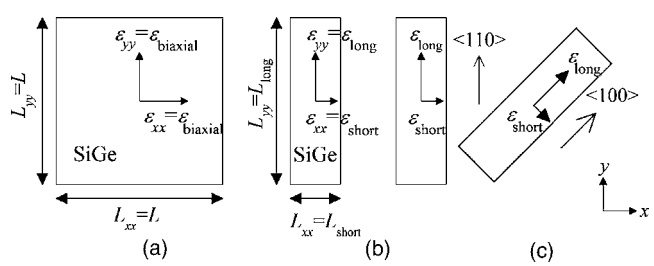

FIG. 2. (a) Top view schematic of a square island, where $L=L_{xx}=L_{yy}$ and at the island center $\varepsilon_{biaxial}=\varepsilon_{xx}=\varepsilon_{yy}$; (b) Top view schematic of rectangular islands and definition of strain directions in the short and long island directions, ε_{short} and ε_{long}, respectively; (c) Schematic of rectangular islands aligned to ⟨100⟩ and ⟨110⟩ crystal directions in the (001) surface plane of the film.

Downloaded 02 Feb 2007 to 128.112.140.109. Redistribution subject to AIP license or copyright, see http://jap.aip.org/jap/copyright.jsp

TABLE I. For silicon and $Si_{0.7}Ge_{0.3}$, values of: deformation potentials, (See Ref. 14) p and q; Raman frequencies for bulk materials, (See Ref. 15) ω_o; elastic stiffness constants, (See Ref. 16) c_{11}, c_{12}, and c_{44}, linearly interpolated between Si and Ge; and elastic compliance constants, s_{11}, s_{12}, and s_{44}, calculated (See Ref. 17) from the stiffness constants. For the ⟨100⟩ crystal direction in the (001) plane, the crystal-direction dependent elastic stiffness coefficients in Eqs. (1) and (6) are related to the given constants by $c'_{11}=c'_{33}=c_{11}$, $c'_{12}=c'_{13}=c_{12}$ and $c'_{44}=c_{44}$. (The prime indicates an arbitary cubic coordinate system.) For other crystal directions, see Ref. 18)

Material	p	q	ω_o (cm^{-1})	c_{11} (10^{10} N/m^2)	c_{12} (10^{10} N/m^2)	c_{44} (10^{10} N/m^2)	s_{11} (10^{-12} m^2/N)	s_{12} (10^{-12} m^2/N)	s_{44} (10^{-12} m^2/N)
Si	−1.85	−2.30	521.0	16.48	6.35	7.90	7.72	−2.15	12.66
$Si_{0.7}Ge_{0.3}$	−1.73	−2.20	501.5	15.39	5.89	7.53	8.24	−2.28	13.27

To obtain asymmetric strain in the plane of the film across entire islands, we choose a rectangular shape for the SiGe islands[7] [Fig. 2(b)]. Because the lateral relaxation time constant depends on the square of island edge length, during relaxation the strains in the two in-plane directions of the rectangle, ε_{short} and ε_{long}, will be different. Upon annealing, the SiGe layer will quickly relax in the short island dimension direction until stress in the short direction σ_{short} equals zero. In contrast, in the long island dimension direction the island maintains its initial strain, $\varepsilon_{long}=\varepsilon_o$, for moderate anneals. Due to the Poisson effect, the SiGe compression in the long direction will create a tensile strain in the short direction[8] (Fig. 3 inset). Thus the short direction of a rectangular island is not fully relaxed as in the square geometry case (where $\varepsilon_{xx}=0$) but is in tension (not compression), with

$$\varepsilon_{\text{short, single SiGe layer}} = -\varepsilon_{long}\nu, \tag{3}$$

where ν is Poisson's ratio of the SiGe film. The strain in the long direction is still ε_o (compression) so that a uniform but highly anisotropic strain results over nearly the entire film. (The uniformity is examined in Sec. III.) Note the difference in the square and rectangular boundary conditions for the single SiGe layer: for the square $\varepsilon_{xx}=\varepsilon_{yy}=\sigma_{xx}=\sigma_{yy}=0$, while for the rectangle, $\sigma_{short}=0$, $\varepsilon_{long}=\varepsilon_o$, and ε_{short}, $\sigma_{long}\neq 0$. The crystal-direction dependence of ε_{short} is the focus of this paper.

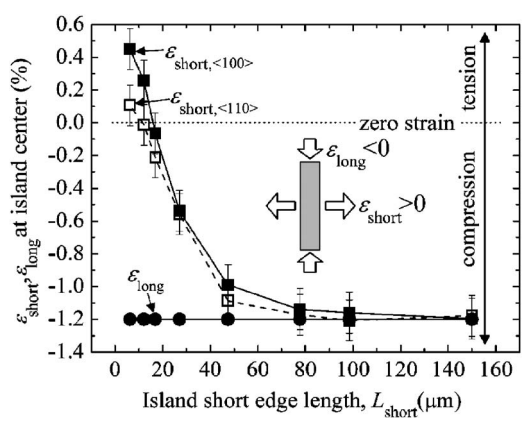

FIG. 3. Measured anisotropic SiGe strain at the center of rectangular islands with $L_{long}=150$ μm vs short island edge length after a 5-min anneal at 750 °C. The layer structure is shown in the Fig. 1 inset. Symbols indicate ε_{short} for islands aligned along ⟨110⟩ (open squares) and along ⟨100⟩ (solid squares); the lines are drawn from point to point. In both cases, ε_{long} (solid circles) is fixed at $\varepsilon_o=-1.2\%$ by the large L_{long} that prevents relaxation. The inset shows a schematic of the Poisson effect acting on a rectangular island: compression in long direction results in extension in the short direction.

Poisson's ratio is strongly dependent on crystal direction. In the (001) plane for a single material, Poisson's ratio is given by[17,18]

$$\nu(\theta) = -\frac{2s_{12} + (s_{11} - s_{12} - s_{44}/2)\sin^2(2\theta)}{2s_{11} - (s_{11} - s_{12} - s_{44}/2)\sin^2(2\theta)}, \tag{4}$$

where θ is the angle with the ⟨100⟩ direction in the (001) plane. The result is plotted in Fig. 4, and for $Si_{0.7}Ge_{0.3}$ in the two directions of interest, takes values of

$$\nu_{\text{SiGe},\langle 100\rangle} = -\frac{s_{12}}{s_{11}} = 0.277$$

$$\text{and } \nu_{\text{SiGe},\langle 110\rangle} = -\frac{s_{11} + s_{12} - s_{44}/2}{s_{11} + s_{12} + s_{44}/2} = 0.054. \tag{5}$$

Thus the highest possible tensile strain (in the direction parallel to the short island edge, ε_{short}) should be achieved with islands aligned to ⟨100⟩, because of the large value of ν in this direction.

To verify this prediction, we pattern islands with a constant L_{long} of 150 μm and various values of L_{short} from 5 to 150 μm. One set of islands is aligned with the edges of the islands parallel to the ⟨100⟩ in-plane crystalline direction while another is aligned to ⟨110⟩, both in the (001) surface plane [Fig. 2(c)]. As in Fig. 1, the islands consist of a single layer of 30-nm $Si_{0.7}Ge_{0.3}$. We perform a relaxation anneal of 5 min at 750 °C and measure the strain at the island center using Raman spectroscopy. From Eq. (2), it is clear that the Raman measured data provide the sum of ε_{xx} and ε_{yy}. For the square island case of biaxial strain, $\varepsilon_{xx}=\varepsilon_{yy}$, and we can

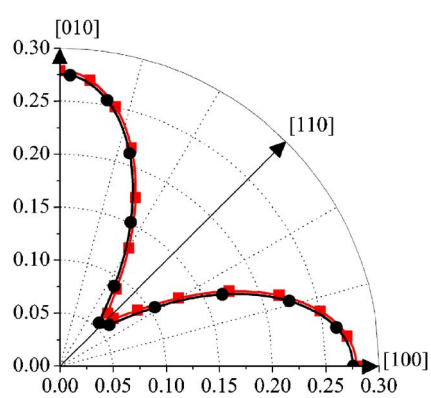

FIG. 4. (Color online) Poisson's ratio ν in silicon (red line with squares) and $Si_{0.7}Ge_{0.3}$ (black line with circles) vs crystal direction in the (001) plane, after Refs. 17 and 18. Symbols are used every six to eight data points to distinguish between the different traces.

Downloaded 02 Feb 2007 to 128.112.140.109. Redistribution subject to AIP license or copyright, see http://jap.aip.org/jap/copyright.jsp

directly obtain the strain values from Raman measurements. For rectangular islands, in order to calculate ε_{short} we assume that ε_{long} is equal to ε_o. This value for ε_{long} can be confirmed by measuring biaxial strain, $\varepsilon_{biaxial}$, for a large square island with edge length equal to the long rectangle dimension under the same annealing conditions, and assuming that the relaxation of the rectangle in the long direction and of the square are equal when $L_{square}=L_{long,rectangle}$. The simulations of Sec. III justify this assumption.

The measured strain in the short island direction is plotted as a function of short island edge length in Fig. 3. The assumed value of $\varepsilon_{long}=\varepsilon_o$ is also plotted. For narrow islands with L_{short} less than 15 μm, the strain in the short direction is tensile as predicted. The narrowest islands, with $L_{short}=6$ μm, have reached the maximum tensile strain state described by Eq. (3), at which $\sigma_{short}=0$. For wider islands with L_{short} greater than 70 μm, the strain in the short direction is still at its initial compressive value ε_o; these islands are large enough that for this short anneal the centers have not yet relaxed. For island sizes between these two extremes, the strain in the short direction is somewhere between ε_o and the maximum tensile ε_{short}, indicating that the relaxation process is in progress.

Figure 3 shows that for narrow rectangular islands, the Poisson effect gives rise to a significant level of tension in the short direction, while the long direction remains compressively strained; the in-plane strain is highly anisotropic. This is contrast to the square island case, in which the equilibrium state is zero in-plane strain, as seen for the smallest island in Fig. 1. Where squares of narrow dimension rapidly become fully relaxed to $\varepsilon_{biaxial}=0$, narrow rectangles quickly become tensilely strained in the short direction, with $\sigma_{short}=0$ and $\varepsilon_{short}=-\varepsilon_o\nu$, while maintaining a compressive strain, $\varepsilon_{long}=\varepsilon_o$, in the long direction. Moreover, for narrow islands where the short direction has reached the zero-stress state, the magnitude of tension in the short direction is strongly dependent on crystal direction. For the narrowest islands shown in Fig. 3, we measure $\varepsilon_{short}=+0.45\%$ and $+0.11\%$ for rectangles aligned to $\langle 100\rangle$ and $\langle 110\rangle$, respectively, in qualitative agreement with our prediction that tension should be maximal in the $\langle 100\rangle$ direction.

Using similar samples, we have also measured the average areal strain over an array of identically sized rectangular islands by x-ray diffraction of the (004) reflection. Typical x-ray diffraction rocking curves and Raman spectra are shown in Fig. 5. As with Raman measurements, in x-ray diffraction we measure average in-plane strain, and assume a value for ε_{long} to calculate ε_{short}. We use three samples—one unpatterned and unannealed, a second patterned into islands but not annealed, and the third patterned and annealed to reach the $\sigma_{short}=0$ state. The measurements show that patterning does not change island strain, but annealing patterned islands has a strong effect as island relaxation takes place. The extracted strain values measured by Raman and x-ray diffraction, tabulated in Table II, agree with one another within the measurement error, confirming the validity of the Raman measurements used throughout this work.

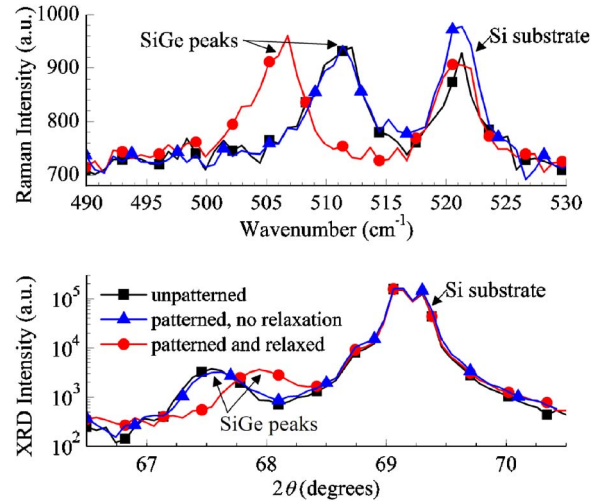

FIG. 5. (Color online) A comparison of micro-Raman spectroscopy and x-ray diffraction measurements of uniaxial strain. The sample is 30-nm $Si_{1-x}Ge_x$ (assumed $x=27\%$) on 95-nm BPSG. On two samples, the SiGe layer is patterned into an array of rectangles 10×8700 μm^2 with 2-μm gaps between the rectangles. One patterned sample is annealed 3.5 h at 900 °C to create uniaxial Si strain. (The viscosity of this BPSG is much higher than that used elsewhere in the paper, thus the high temperature and lengthy anneal.) Raman spectroscopy is performed at 514 nm with ~3 μm laser spot size, and displays a silicon substrate peak around 521 cm^{-1}, with the SiGe peak between 500 and 515 cm^{-1}. X-ray diffraction was done with the sample spinning, as for powder measurements. The double peaks around $2\theta=69°$ are the first and second Cu $K\alpha$ peaks from the silicon substrate, while the peaks from $2\theta=67°-68.5°$ are from SiGe. Symbols are placed every four to five data points to distinguish between the different traces.

III. DYNAMIC MODEL AND PROCESS WINDOW FOR GENERATION OF ANISOTROPIC STRAIN

In this section we examine the rate at which a single layer of a compressively strained film (i.e., SiGe) relaxes for both square and rectangular island geometries. For squares, the in-plane lateral expansion process has been modeled in Ref. 11 and compared to experimental data in Ref. 10. Here we extend that model to rectangular islands, and determine process windows for maximum asymmetry of strain. We model the case of islands aligned to the $\langle 100\rangle$ crystal direction. For other crystal directions, the general conclusions re-

TABLE II. Strain in the short island direction ε_{short} under various conditions, extracted from the raw data shown in Fig. 5. Unpatterned and patterned samples with no anneal have the original compressive strain ε_o of approximately −1.2%. Patterned samples that have been annealed show a small amount of tensile strain, +0.1%, in the short island direction, as expected when $\sigma_{short}=0$ for islands aligned to $\langle 110\rangle$. A full description of the samples is given in the Fig. 5 caption. For each sample, the Raman and x-ray results agree within the measurement error of approximately ±0.1%, although some disagreement is to be expected as Raman measures strain at the island center whereas x-ray diffraction measures areally averaged strain.

	Strain in the short island direction, ε_{short}, measured by	
Sample	Micro-Raman spectroscopy	X-ray diffraction
Unpatterned	−1.16%	−1.18%
Patterned, with no anneal	−1.19%	−1.11%
Patterned and annealed	+0.06%	+0.10%

Downloaded 02 Feb 2007 to 128.112.140.109. Redistribution subject to AIP license or copyright, see http://jap.aip.org/jap/copyright.jsp

main the same, but the values of the direction-dependent elastic stiffness coefficients in Eqs. (1) and (6) change as specified in Ref. 18. For silicon or SiGe islands aligned to the ⟨110⟩ direction, this results in a ~15% reduction in τ_L, and a reduction in the maximum asymmetry of strain, that is, a lower tensile strain in the short island direction for the same compressive strain in the long direction, as described by Eqs. (3)–(5).

The BPSG glass layer is assumed to be linearly viscous, with flow velocity linear from the bottom to the top surface. We assume that the single layer film (SiGe) and BPSG expand together at their interface, and that the film stays flat during lateral expansion, with the film surface in the (001) plane. The displacement of the film u in the short direction x and the displacement of the film v in the long direction y as a function of time t are defined by two diffusion equations:[11]

$$\frac{\partial u}{\partial t} = \frac{c'_{11} h_f h_g}{\eta}\left[\left(1 - \frac{c'^2_{13}}{c'_{11}c'_{33}}\right)\frac{\partial^2 u}{\partial x^2} + \left(\frac{c'_{44}}{c'_{11}}\right)\frac{\partial^2 u}{\partial y^2} + \left(\frac{c'_{12}+c'_{44}}{c'_{11}} - \frac{c'^2_{13}}{c'_{11}c'_{33}}\right)\frac{\partial^2 v}{\partial x \partial y}\right], \tag{6a}$$

$$\frac{\partial v}{\partial t} = \frac{c'_{11} h_f h_g}{\eta}\left[\left(1 - \frac{c'^2_{13}}{c'_{11}c'_{33}}\right)\frac{\partial^2 v}{\partial y^2} + \left(\frac{c'_{44}}{c'_{11}}\right)\frac{\partial^2 v}{\partial x^2} + \left(\frac{c'_{12}+c'_{44}}{c'_{11}} - \frac{c'^2_{13}}{c'_{11}c'_{33}}\right)\frac{\partial^2 u}{\partial x \partial y}\right]. \tag{6b}$$

Clearly these equations are directly linked to the definition of the lateral relaxation time constant in Eq. (1); the coefficient on the right side of the equations $c'_{11}h_f h_g/\eta$ is equal to $\tau_L^{-1}L^2$. The local strain is calculated as

$$\varepsilon_{xx}(x,y,t) = \varepsilon_{\text{short}}(x,y,t) = \frac{\partial u(x,y,t)}{\partial x} + \varepsilon_o, \tag{7a}$$

$$\varepsilon_{yy}(x,y,t) = \varepsilon_{\text{long}}(x,y,t) = \frac{\partial v(x,y,t)}{\partial y} + \varepsilon_o. \tag{7b}$$

Boundary conditions require that at the island edges, the in-plane stresses are zero. Eqs. (6a) and (6b) can be solved numerically using the finite difference method for the in-plane displacements, $u(x,y,t)$ and $v(x,y,t)$, and the strains calculated directly from Eqs. (7a) and (7b).

Plots of cross-sectional normalized strain $\varepsilon/\varepsilon_o$, versus normalized anneal time t/τ_L are shown in Fig. 6 for a single $Si_{0.7}Ge_{0.3}$ layer that is initially fully compressively strained. Strain and time values are normalized so that these simulations may be applied to arbitrary structures. The vertical axis indicates normalized strain, with 1.0 being fully compressive ($\varepsilon=\varepsilon_o$), zero being unstrained ($\varepsilon=0$), and negative numbers indicating tension. From Eq. (3), the maximum normalized tension is equal to $-\nu$, and thus depends on the film material properties and island crystal direction. In the top plot, Fig. 6(a), square island edges quickly relax and gradually the center also relaxes. The final state is zero strain across the island. Similar results were shown in Ref. 11 for squares, and are repeated here to contrast with the result for rectangular islands. In the middle plot, normalized strain across the short

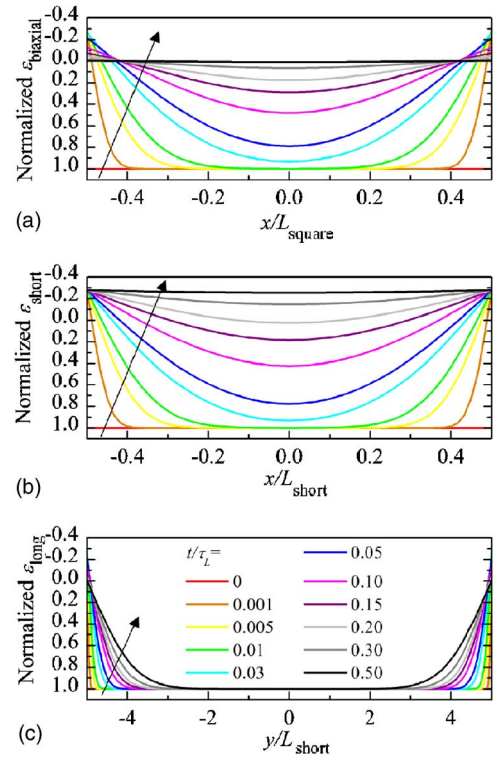

FIG. 6. (Color online) Numerical simulations of the strain across an island cross section for various anneal times. The plots show cross sections of: (a) a square island, (b) the short direction, and (c) the long direction of a rectangular island with $L_{\text{long}}=10L_{\text{short}}$ (note the different horizontal axis scales). The islands simulated are a single $Si_{0.7}Ge_{0.3}$ layer initially fully compressively strained, aligned to ⟨100⟩. The strain, plotted on the vertical axis, is normalized so the initial compressive strain equals 1.0. Each line represents a different anneal time t, normalized by τ_L, the lateral relaxation time of Eq. (1). In the directions of the arrows, the t/τ_L values are 0, 0.001, 0.005, 0.01, 0.03, 0.05, 0.1, 0.15, 0.2, 0.3, and 0.5.

dimension of a rectangle is plotted (for comparison purposes, τ_L is calculated with $L=L_{\text{short}}=L_{\text{square}}$). The curves look similar to those of the square, but this time the final simulation point indicates uniform tension in the short direction equal to $-\nu$. The bottom plot shows strain across the long dimension of the same rectangle, where $L_{\text{long}}=10L_{\text{short}}$. Again, the strain gradually relaxes with time. However, for the longest time simulated, the majority of the island still remains fully compressively strained in the long direction. At the last simulation point, $t/\tau_L=0.5$, the strain across the rectangular island is quite uniform: over the entire short direction, the tensile strain is uniform within 9%, while over the central 70% of the long direction, the compressive strain is uniform within 10%. Thus, our dynamic model precisely agrees with the Poisson theory (which predicts only the end point): a biaxially strained SiGe layer, patterned into a rectangle and annealed, will have compression in the long direction and tension in the short direction. Supplemental Figs. 1 and 2 have full three-dimensional (3D) simulation images of the strain relaxation process for squares and rectangles, respectively.

So far, we have discussed only very narrow, long rectangular islands. For such structures, the anisotropic strain state will persist for quite long anneals. However, eventually the long island direction will begin to relax. We should emphasize that the final equilibrium state for all island shapes

Downloaded 02 Feb 2007 to 128.112.140.109. Redistribution subject to AIP license or copyright, see http://jap.aip.org/jap/copyright.jsp

and sizes is the same: full relaxation in both in-plane directions. Clearly, the aspect ratio of the rectangle (defined as L_{long}/L_{short}) plays a critical role in determining the existence and length of a process window for maximum anisotropy of strain and, as discussed in Sec. IV, uniaxial silicon strain. To investigate, numerical simulations of lateral relaxation were performed using Eqs. (6) and (7) for rectangles with various aspect ratios. In Fig. 7(a), strain at the island center is plotted versus anneal time for rectangular islands with aspect ratios of 3 and 5, and for square islands. Initially, the rectangular islands generate highly asymmetric strain, with the long direction maintaining initial compressive strain and the short direction becoming tensile. As the anneal progresses, the compressive strain in the long direction begins to relax to zero. As this occurs, the driving force for tension in the short direction is removed, and the tensile strain in the short direction also relaxes toward zero. Eventually, ε_{short} and ε_{long} for rectangles converge to the same value as $\varepsilon_{biaxial}$, for squares—both the long and short directions fully relax to zero strain (and zero stress). The higher the aspect ratio of the island rectangle, the longer the process window before such convergence occurs.

A desirable technological goal is to achieve maximum asymmetry of strain in the two in-plane directions. We define this as ε_{short}-ε_{long} and plot it normalized by ε_o for various rectangular island aspect ratios in Fig. 7(b). For squares, there is never any asymmetry: ε_{short}-$\varepsilon_{long} \equiv 0$. For rectangles, the strain asymmetry increases as the short direction relaxes, and then as the long direction relaxes, the asymmetry decreases to zero. For rectangular islands with aspect ratios of 5 or more, the maximum possible asymmetry of ε_{short}-$\varepsilon_{long} = -(1+\nu)\varepsilon_o$ is achievable before the asymmetry falls to zero. A process window for maximum strain asymmetry then exists: for an island with an aspect ratio of 5, the strain asymmetry is at least 90% of its maximum value from $t/\tau_L = 0.30-1.04$, as seen in Fig. 7(b). As the island aspect ratio increases, this process window widens significantly. For an aspect ratio of 10, a process window for 90%+ strain asymmetry exists from $t/\tau_L = 0.30$ to $t/\tau_L > 4.0$. However, if an island has a smaller aspect ratio, the long and short sides are too close in length, relaxing on similar time scales, so it is difficult to exploit the L^2 dependence of τ_L that drives strain asymmetry. In Fig. 7(b) this is shown by the curves for aspect ratios 3.0, 1.867, and 1.5, which never reach the maximum asymmetry value. For an island with the cross section shown in the Fig. 1 inset, with $L_{long} = 150\ \mu m$ and $L_{short} = 30\ \mu m$, our model predicts a generous process window yielding greater than 90% of the maximum asymmetric strain for 750 °C anneals between 0.9 and 3.1 h in length.

Finally, these simulation results are compared to the measured biaxially symmetric and asymmetric SiGe strain plotted in Figs. 1 and 8, respectively. Solid lines represent modeled strains at the island center. The Raman measurement has a finite beam spot size (~3 μm) and thus for small islands the measured and predicted results diverge for $\varepsilon_{biaxial}$ (in Fig. 1) and ε_{short} (in Fig. 8). The generally good agreement of the dynamic model and experimental data for both square and rectangular islands demonstrates the high level of control and predictability that our strain generation process affords. The model predicts that for the given anneal all islands are characterized by $\varepsilon_{long} = \varepsilon_o$, which justifies using this assumption in analyzing the Raman data to calculate ε_{short} as described above in Sec. II.

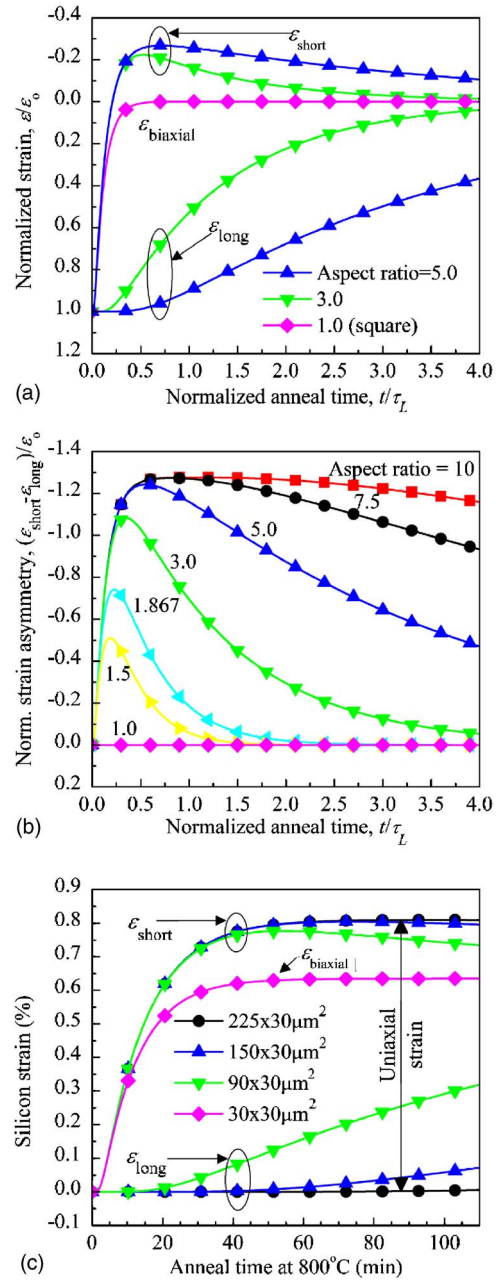

FIG. 7. (Color online) (a) Normalized strain $\varepsilon/\varepsilon_o$ for a single SiGe layer vs normalized anneal time t/τ_L where τ_L is calculated from Eq. (1) with $L = L_{short} = L_{square}$. Shown in the plot are strain in the short direction ε_{short} and strain in the long direction ε_{long} for rectangles with aspect ratios of 3 and 5, and biaxial strain $\varepsilon_{biaxial}$ for a square island. At long times, ε_{short} and ε_{long} converge at $\varepsilon_{biaxial}$. (b) Normalized strain asymmetry $(\varepsilon_{short}-\varepsilon_{long})/\varepsilon_o$ vs normalized anneal time. Strain asymmetry for a single SiGe layer is plotted for rectangular islands with different aspect ratios. Aspect ratios of 5 or more are needed to obtain maximum asymmetry of strain; (c) Model of uniaxial and biaxial silicon strain development as a function of anneal time at 800 °C for rectangular islands with different aspect ratios, aligned to ⟨100⟩, and for a square island. The island cross section is shown in the Fig. 10 inset. Uniaxial in-plane silicon strain, for which ε_{short} is maximum while ε_{long} is close to zero, is indicated. For (a)–(c), the plots show strain at the island center. Symbols are placed every ~1000 data points to distinguish the different traces.

Downloaded 02 Feb 2007 to 128.112.140.109. Redistribution subject to AIP license or copyright, see http://jap.aip.org/jap/copyright.jsp

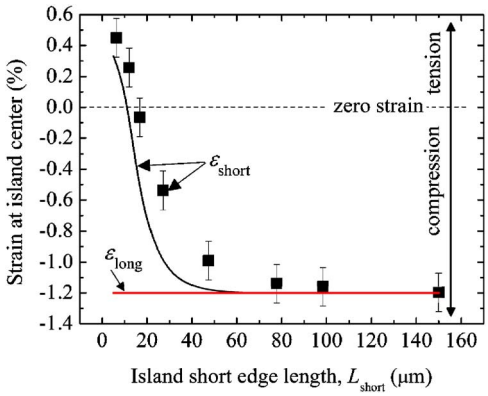

FIG. 8. (Color online) Comparison of Raman measurements with model predictions of SiGe strain at the island center. Symbols indicate measured values of ε_{short} for rectangular islands aligned to ⟨100⟩ (data is identical to Fig. 3 with the layer structure of Fig. 1 inset). The solid lines are predicted strains ε_{short} and ε_{long}, as marked.

IV. UNIAXIAL STRAIN IN SI AND ITS CRYSTAL-DIRECTION DEPENDENCE

In this section we build on the earlier work in this paper to show the crystal-direction dependence of uniaxial strain in silicon, by substituting a SiGe/Si bilayer for the single SiGe layer previously used.

An unstrained silicon cap, of comparable thickness to the SiGe layer, is grown on top of the SiGe during initial epitaxy. The silicon and BPSG surfaces are then bonded and the SiGe/Si bilayer stack transferred to the BPSG handle wafer. After layer transfer the SiGe remains fully compressively strained with $\varepsilon_o=-1.2\%$, and the underlying silicon layer remains unstrained (see Fig. 10 inset for cross section). When at high temperature the BPSG softens, the SiGe becomes less-compressively strained. As the SiGe layer relaxes it stretches the silicon layer to make it tensile. The SiGe and silicon layers have been shown to remain coherent, so that the structure acts like a perfect "virtual substrate"[19] and no misfit dislocations are required to generate the strain in the silicon layer. In Fig. 9, the strain in both layers after a brief anneal is plotted versus position along a cross section of the

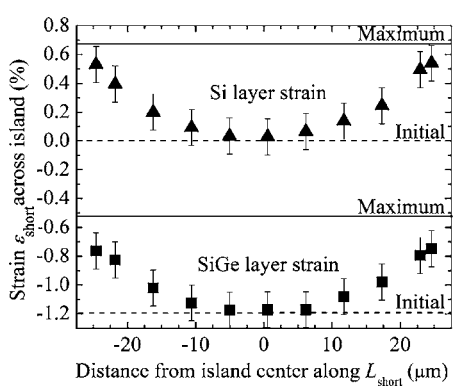

FIG. 9. Measured strain in the short island direction, ε_{short}, across a 50 $\times 150\ \mu m^2$ island aligned along ⟨110⟩ after a 15-min anneal at 750 °C. Figure 10 inset shows the SiGe/Si bilayer structure. The relaxation begins at the edges of the island and proceeds toward the center, which for this short anneal remains in the initial, fully strained state. The change in strain is identical for the Si (triangles) and SiGe (squares) films, showing that the film interface is coherent.

TABLE III. Coefficients to calculate film strain in the short island direction from Eq. (9). The values s_{11}, s_{12}, and s_{44} refer to compliance coefficients (Table I) and ν is Poisson's ratio [Eqs. (4) and (5)]. Theta, θ, is the angle the island edges make with the ⟨100⟩ direction in the (001) plane.

Strain type	Condition on ε_{long}	A	B
Biaxially symmetric	$\varepsilon_{long}=\varepsilon_{short}$	1	$\frac{s_{11,SiGe}+s_{12,SiGe}}{s_{11,Si}+s_{12,Si}}$
Asymmetric, edges aligned to θ	$\varepsilon_{long}=\varepsilon_{initial}$	$\frac{1}{1+\nu_{SiGe}(\theta)}$	$\left(\frac{s_{11,SiGe}+s_{12,SiGe}}{s_{11,Si}+s_{12,Si}}\right)\left[\frac{1}{1+\nu_{Si}(\theta)}\right]$

short dimension of a rectangular island. The nature of lateral expansion is evident: the edges are close to the maximum strain values, while the middle of the island remains in its initial strain state. The coherence of the SiGe/Si film interface is demonstrated by the identical change in strain for the SiGe and silicon layers, shown in Fig. 9.

Upon a longer anneal, the two layers reach an equilibrium state of stress balance, at which

$$\sigma_{Si}h_{Si} + \sigma_{SiGe}h_{SiGe} = 0, \tag{8}$$

where σ is the stress and h the thickness of each layer.[7,19] Here, we assume that the layers remain flat without curling. Note that for single layers, the boundary condition was defined as the zero stress case, $\sigma=\varepsilon=0$, whereas for a bilayer the equilibrium film stresses are nonzero and must be calculated from Eq. (8). In both cases, equilibrium occurs at the minimum energy state, when there is no net force to drive further relaxation.

For a rectangular bilayer island, the strain in the short direction ε_{short} of rectangular islands has two contributions: (1) the stress balance of the bilayer; and (2) the asymmetry of the rectangular island (the Poisson effect). To calculate the short direction strain for bilayers, Eq. (3), which is valid for single layers, is too simplistic. Instead, the stress balance model of Eq. (8) is solved assuming that the long island directions maintain their initial strain ($\varepsilon_{long,SiGe}=\varepsilon_o$; ε_{long}, Si=0). The result is

$$\varepsilon_{short,Si} = \frac{-\varepsilon_o}{A(\theta) + B(\theta)h_{Si}/h_{SiGe}}, \tag{9}$$

where A and B are given in Table III, and are functions of the island geometry (square or rectangular), and the crystal direction alignment, θ, of the island (e.g., $\theta=0°$ for ⟨100⟩ and $\theta=45°$ for ⟨110⟩). From Table III, it is clear that A and B for rectangular geometries are smaller, by factors of $(1+\nu)$, than A and B for square geometries. Physically, the silicon tension from the Poisson effect adds to the tension generated by stress balance, so the uniaxial silicon tensile strain for rectangular islands will always be greater than biaxial tensile strain generated in square islands. The crystal-direction dependence of Poisson's ratio means that maximum uniaxial silicon tension occurs in the ⟨100⟩ direction:

Downloaded 02 Feb 2007 to 128.112.140.109. Redistribution subject to AIP license or copyright, see http://jap.aip.org/jap/copyright.jsp

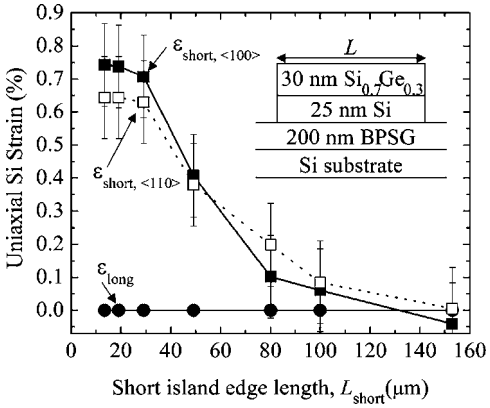

FIG. 10. Measured uniaxial silicon strain in rectangular islands with L_{long} =150 μm vs short island edge length after a 30-min anneal at 800 °C. The layer structure is shown in the inset. Symbols indicate ε_{short} for islands aligned along ⟨100⟩ (solid squares) and along ⟨110⟩ (open squares), with lines drawn from point to point. In both cases, ε_{long} (solid circles) is fixed at zero by the large L_{long} that prevents relaxation.

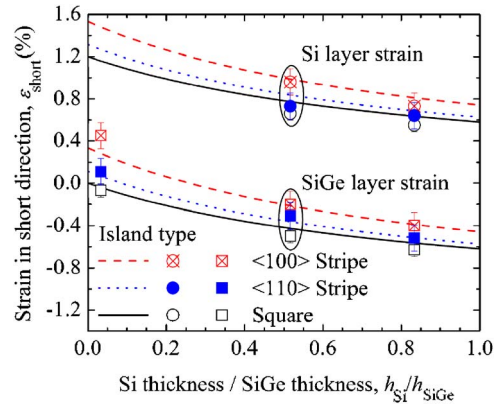

FIG. 11. (Color online) Silicon and SiGe strain in the short direction vs the film thickness ratio h_{Si}/h_{SiGe}. Lines are the combined force balance and asymmetry model of Eq. (9) and Table II, while symbols are measured data. The open symbols and solid line indicate square islands; solid symbols and dotted line indicate rectangular islands along ⟨110⟩; and crosshatched symbols and dashed line indicate rectangular islands along ⟨100⟩. The leftmost data points correspond to Fig. 1 inset, the rightmost data to Fig. 10 inset, and the middle data to a sample with 30-nm $Si_{0.7}Ge_{0.3}$ on 10-nm Si on 5.5-nm SiN_x on 1-μm BPSG.

$$\varepsilon_{\text{uniaxial,Si}\langle 100\rangle} > \varepsilon_{\text{uniaxial,Si}\langle 110\rangle} > \varepsilon_{\text{biaxial,Si}}. \tag{10}$$

Since the two layers are coherent, the SiGe strain is simply $\varepsilon_{SiGe}=\varepsilon_{Si}+\varepsilon_o$.

The experiment described in Sec. II to obtain anisotropic strain in a single SiGe layer is repeated with a SiGe/Si bilayer to generate uniaxial silicon strain after Ref. 7. The results are shown in Fig. 10. The silicon layer is uniaxially strained in the surface plane: in the short direction there is a high level of tension (+0.6% to +0.8% strain as shown in Fig. 10), while in the long direction the silicon remains unstrained. As predicted, rectangular islands aligned to ⟨100⟩ show the maximum amount of tension, and uniaxial strain in both ⟨100⟩ and ⟨110⟩ are greater than the measured maximum biaxial strain of +0.54%.

In Fig. 11, the experimental data for several samples are compared to the stress balance model of Eq. (9), and excellent agreement is seen. Using our strain generation process, the maximum uniaxial silicon tensile strain achieved to date is +1.0% (circled data pts in Fig. 11). This strain is obtained on a structure of 30 nm $Si_{0.7}Ge_{0.3}$–10 nm Si–5.5 nm SiN_x –1 μm BPSG, where the nitride layer is inserted to prevent outdiffusion[6] of boron and phosphorous from BPSG into the Si/SiGe. For Si/SiGe bilayers, after annealing to generate silicon strain, the SiGe can be removed by selective etch to leave an ultrathin (~25 nm) uniaxially or biaxially strained silicon-on-insulator structure, ideal for device fabrication.

Finally, the simulations described in Sec. III can be used to predict process windows for uniaxially strained silicon, as shown in Fig. 7(c), by using the known maximum strain asymmetry [from Eq. (9)] and relaxation time constant[12] for the SiGe/Si bilayer to linearly scale the normalized strain and time scales calculated in Sec. III. For islands with high aspect ratios, there exist processing windows for maximum uniaxial silicon strain. For a rectangle of dimensions 225 ×30 μm^2 with the structure shown in the Fig. 10 inset, the predicted uniaxial silicon strain is at 90% or more of its maximum value of +0.81% for 800 °C anneals from 31 min to 4 h in length as shown in Figs. 7(b) and 7(c). If the island has a small aspect ratio or is annealed beyond the uniaxial strain process window, ultimately both "long" and "short" strains would converge at the biaxial strain value determined by stress balance, indicated for a 30×30 μm^2 square island in Fig. 7(c).

While the biaxial and uniaxial silicon strain generation processes have been developed here for islands with large areas (~100–1000 μm^2), one can think about scaling islands down to sizes appropriate for individual devices. For such an approach, the channel width would be aligned in the long rectangle direction, with the length in the short direction. This would yield uniaxial tensile silicon strain in the direction from source to drain, as conventionally sought in device technology.[2] The smaller island sizes would require anneals at lower temperature or increased BPSG viscosity, or a reduced BPSG thickness. Extrapolating from known viscosity values assuming exponential $1/T$ behavior with E_A =2.9 eV, uniaxial silicon strain for 0.1×1 μm^2 islands on 200 nm BPSG (Fig. 10 cross section) would be maximized after an anneal of 1–6 min at 600 °C. Further experimental work and modeling are needed to investigate the effect of the silicon area required for source/drains and the effect of short-channel FET processing on the strain stability.

V. CONCLUSION

The generation of uniaxial strain in silicon and SiGe is of major interest due to the ability of certain types of strain to enhance electron and hole mobility. Here we have presented a strain generation technique that allows for the integration of multiple strain types and crystal directions on a single sample. We have demonstrated uniaxial silicon strain of up to 1.0%, and have shown that uniaxial strain made by this lateral expansion method is maximal in the ⟨100⟩ direction. Finally, we have presented dynamic and static models that allow precise prediction and control of the strain generation process. Work is ongoing to measure the electron and hole mobility in these strained layers.

Downloaded 02 Feb 2007 to 128.112.140.109. Redistribution subject to AIP license or copyright, see http://jap.aip.org/jap/copyright.jsp

ACKNOWLEDGMENTS

Many thanks to R. Huang of University of Texas at Austin for providing the numerical calculation script for square islands and to A. Margarella of Northrop Grumman for BPSG deposition. This work was supported by grants from the Office of Naval Research/Defense Advanced Research Projects Agency (Grant No. N66001-00-1-8957), the Army Research Office (Grant No. DAA655-98-1-0270), and Applied Materials, Inc., and by an Engineering Dissertation Fellowship from the American Association of University Women.

[1]K. Rim *et al.*, Digest of Technical Papers, 2001 Symposium on VLSI Technology, 12–14 June, 2001, 59–60.
[2]S. E. Thompson *et al.*, IEEE Trans. Electron Devices **51**, 1790 (2004).
[3]T. Guillaume, M. Mouis, S. Maîtrejean, A. Poncet, M. Vinet, and S. Deleonibus, Proceedings of the 2004 IEEE International SOI Conference, 4–7 October 2004, 42–43.
[4]B. M. Haugerud, L. A. Bosworth, and R. E. Belford, J. Appl. Phys. **94**, 4102 (2003).
[5]H. R. Kirk, I. J. Malik, J. Sullivan, S. Kang, A. J. Lamm, P. J. Ong, and F. J. Henley, Proceedings of the 2004 IEEE International SOI Conference, 4–7 October 2004, 2004, 102–103.
[6]H. Yin, K. D. Hobart, R. L. Peterson, F. J. Kub, and J. C. Sturm, IEEE Trans. Electron Devices **52**, 2207 (2005).
[7]H. Yin, K. D. Hobart, R. L. Peterson, S. R. Shieh, T. S. Duffy, and J. C. Sturm, Appl. Phys. Lett. **87**, 061922 (2005).
[8]R. L. Peterson, K. D. Hobart, H. Yin, and J. C. Sturm, Proceedings of the 2004 IEEE International SOI Conference, 4–7 October 2004, 2004, 39–41.
[9]K. D. Hobart, F. J. Kub, M. Fatemi, M. E. Twigg, P. E. Thompson, T. S. Kuan, and C. K. Inoki, J. Electron. Mater. **29**, 897 (2000).
[10]H. Yin *et al.*, J. Appl. Phys. **91**, 9716 (2002).
[11]R. Huang, H. Yin, J. Liang, K. D. Hobart, J. C. Sturm, and Z. Suo, Mater. Res. Soc. Symp. Proc. **695**, 115 (2002).
[12]H. Yin, R. Huang, K. D. Hobart, J. Liang, Z. Suo, S. R. Shieh, T. S. Duffy, F. J. Kub, and J. C. Sturm, J. Appl. Phys. **94**, 6875 (2003).
[13]See EPAPS Document No. E-JAPIAU-100-276612 for figures showing 3D images of strain in square and rectangular islands vs relaxation anneal time. The document can be reached via a direct link in the online article's HTML reference section or via the EPAPS homepage (http://www.aip.org/pubservs/epaps.html). Note that during the relaxation process the SiGe strain is only biaxially symmetric at the island center. For example, at the island edge the film stress perpendicular to the edge is zero while the stress parallel to the edge is nonzero, leading to asymmetric biaxial strain, as shown in the images of ε_{xx} and ε_{yy} in supplemental Fig. 1. Of course, the strain is biaxially symmetric across the entire island both before annealing (full initial biaxial strain), and at the end of a long anneal (full relaxation, zero strain).
[14]S. C. Jain, B. Dietrich, H. Richter, A. Atkinson, and A. H. Harker, Phys. Rev. B **52**, 6247 (1995).
[15]J. C. Tsang, P. M. Mooney, F. Dacol, and J. O. Chu, J. Appl. Phys. **75**, 8098 (1994).
[16]M. Neuberger, *Group IV Semiconducting Materials*, Handbook of Electronic Materials Vol. 5 (IFI/Plenum, New York, 1971).
[17]W. A. Brantley, J. Appl. Phys. **44**, 534 (1973).
[18]J. J. Wortman and R. A. Evans, J. Appl. Phys. **36**, 153 (1965).
[19]H. Yin, K. D. Hobart, F. J. Kub, S. R. Shieh, T. S. Duffy, and J. C. Sturm, Appl. Phys. Lett. **82**, 3853 (2003).

Downloaded 02 Feb 2007 to 128.112.140.109. Redistribution subject to AIP license or copyright, see http://jap.aip.org/jap/copyright.jsp